Spiral Patterns in the Packing of Flexible Structures

L. Boué, M. Adda-Bedia, A. Boudaoud,* D. Cassani, Y. Couder, A. Eddi, and M. Trejo

Laboratoire de Physique Statistique de l'Ecole Normale Supérieure, 24 Rue Lhomond, 75231 Paris Cedex 05, France

(Received 20 July 2006; published 20 October 2006)

Spiral patterns are found to be a generic feature in close-packed elastic structures. We describe model experiments of compaction of quasi-1D sheets into quasi-2D containers that allow simultaneous quantitative measurements of mechanical forces and observation of folded configurations. Our theoretical approach shows how the interplay between elasticity and geometry leads to a succession of bifurcations responsible for the emergence of such patterns. Both experimental forces and shapes are also reproduced without any adjustable parameters.

DOI: 10.1103/PhysRevLett.97.166104 PACS numbers: 68.55.−a, 46.32.+x, 46.65.+g

Illustrations of tightly packed flexible structures abound in nature from plant leaves in buds [1], insect wings in cocoons [2], DNA in viral capsids [3], chromatin in cell nuclei [4] to crumpled sheets [5–14] and rods [15–17]. This situation is often a consequence of the structures' own growth within a container or of a decrease in the available volume. In most cases the geometrical arrangement of the folding plays a central role in ensuring a safe deployment [1,4]. Besides, the elastic properties of these confined systems are further constrained by self-avoidance as well as by the dimensionality of both structures and containers. The interplay of these mechanisms usually yields a variety of possible self-organized patterns [1–17]. Their complexity led to approaches separating elastic forces [5,7–11,17] and geometrical configurations [6,16,18,19]. So far, in experiments on crumpled thin sheets [6,11,12] and rods [16], it has remained elusive to simultaneously determine mechanical forces and the corresponding configurations. Here, we make these measurements possible with an intermediate approach: the quasi-two-dimensional confinement of thin sheets. Ideally, this would correspond to the folding of an elastic rod when it is confined isotropically in a disk of decreasing radius, or equivalently when an elastic rod grows within a disk of fixed radius. We identify spirals as the building block of the apparently complex patterns observed and study in detail the generation of an isolated spiral. In parallel, our theoretical approach accounts for both elasticity and self-avoidance and agrees quantitatively with experiments.

Our first experimental setup, designed in a *conical geometry*, is inspired by the one used to study single developable cones [8,9]. A circular sheet of typical radius 40 cm and thickness $h = 0.1$ mm is pulled through a circular rigid hole of radius R of the order of 1 cm [Fig. 1(a)]. The distance Z between the pulling point and the plane of the hole serves as a control parameter. As it is much easier to bend the sheet than to stretch it, the sheet first assumes the shape of a developable cone, except near the tip where the pulling force is applied. This setup allows a quasi-one-dimensional, isotropic confinement as: (i) a cut across the sheet in the plane of the hole yields a rodlike one-dimensional structure of length $L = 2\pi Z$, which grows within a disk of radius R as Z is increased—the shape of the cross section actually prescribes the shape of the whole sheet due to the approximately self-similar conical shape.

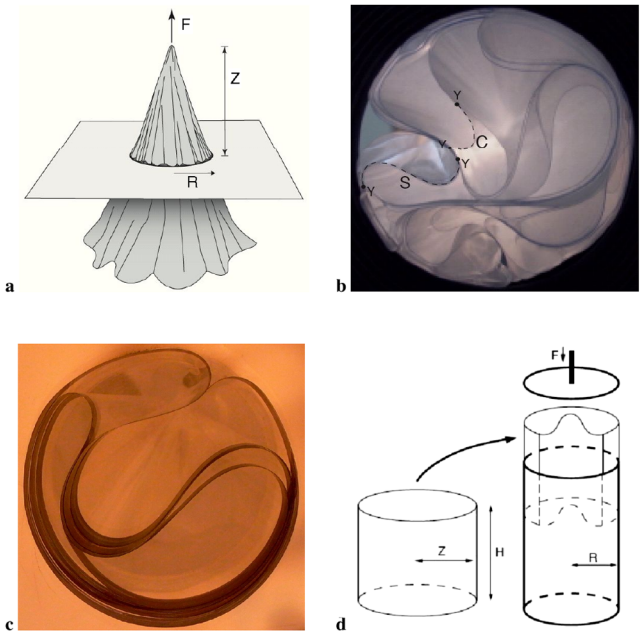

FIG. 1 (color online). Experimental setups and patterns. We used Mylar sheets of thickness $h = 0.1$ mm and bending modulus $B = 6.610^{-4}$ N m. (a) Setup for conical packing. A sheet of radius 40 cm is pulled through a hole of radius 1 cm. (b) Typical pattern at high confinement ($p = 15\%$). Examples of Y points (bifurcations), C curves, and S curves are shown. (c) Typical pattern at lower confinement ($p = 3\%$). A double-layered S curve inside a set of C curves forming a smaller effective container. (d) Setup for cylindrical packing. Sheets of height $H = 14$ cm are glued into a cylinder and introduced into a Plexiglass container of inner radius $R = 2.6$ cm and height 38 cm. The sheet is pushed at small velocity ($0.5\ \mathrm{mm\,s^{-1}}$) with an aluminum disc of radius 5 cm, and the pushing force F is recorded in a steady state (results in Fig. 3).

(ii) It is ensured that there is no preferred direction in the disk.

The strength of the confinement can be measured using the ratio of a cross-sectional area to that of the hole $p = Lh/S$ with $S = \pi R^2$. When most of sheet has been pulled through the hole, the packing fraction p can be as large as 20%. Figure 1(b) shows a deceivingly complex shape typically observed for high confinements. However, a careful glance allows one to abstract out some much simpler well-defined patterns: (i) Y points where a stack of layers bifurcates tangentially into two groups; (ii) curves connecting Y points, which can themselves be classified into two types: C curves and S curves (with and without inflexion points, respectively).

Generically, S curves appear to link concave C curves acting as a flexible shell smaller than the outer rigid disk. These observations suggest that in order to understand close packing, one should focus on the generation of these elementary patterns. It is possible to isolate them during the early stages of the packing process and Fig. 1(c) shows an S curve, assuming a yin-yang-like shape, enclosed in a container formed of stacks of three C curves. While the pressure exerted on the container could be related to the pulling force F, friction on the container and configurational changes are mixed up, which results in a rather circumvoluted interpretation of F.

Thanks to Ref. [17], we know that conical and cylindrical geometries are described by the same equations except for some slightly different developability constraints. Besides, for large confinements, a slender cone is obviously equivalent to a cylinder. Therefore, we devised a second experimental setup designed in a *cylindrical geometry*. A sheet of height H and width L is glued into a cylinder of radius $Z = L/2\pi$. With its configuration prepared according to the topologies observed in the conical geometry, the sheet is introduced inside a smaller cylindrical container of radius R and let to relax to an equilibrium shape by tapping in order to minimize the effect of friction at the lineic self-contacts. Then the folded sheet is pushed along the inside of the container [Fig. 1(d)]. The pushing force F is recorded when a steady state is reached. Because F is proportional to the mean pressure P exerted on the container through Coulomb's law: $F = \mu 2\pi RHP$, this new setup achieves the goal of simultaneous observation of configurations and measurement of pressures. The dynamic friction coefficient $\mu = 0.37$ between the sheet and the container was measured independently.

The classical theory of bending due to Bernoulli and Euler stands as a cornerstone in elasticity theory. Within this framework, the mechanical properties and the shape of rods and cylindrical sheets can be determined by solving the equation of Euler's *Elastica*:

$$B\left[\frac{d^2\kappa}{ds^2} + \left(a^2 + \frac{1}{2}\kappa^2\right)\kappa\right] = k, \qquad (1)$$

where κ is the curvature of the rod at arclength s, B is the bending modulus, a is an undetermined constant of integration, and k represents the external normal forces. However, the obvious physical constraint of self-avoidance gives rise to many complications in the prescription of suitable boundary conditions. Also, since the position and nature of these contacts is not known *a priori*, the formulation results in a nonlinear free-boundary problem. The boundary conditions necessary to close this formulation are determined at all n Y points that may be present in the rod and can be separated into two kinds: (i) *local mechanical equilibrium.* Because of torque and tangential forces equilibrium, the curvature κ is continuous all along the rod and the constants a_i $\{i = 1, \ldots, n\}$ satisfy simple algebraic relations. The exact form of these compatibility equations depends on the nature of the Y point considered (localized or extended contact between curves) but always stems from tangential forces equilibrium. On the other hand, normal forces are proportional to local changes in curvature and provide a set of relations between the values of the curvature derivative κ' just before and after Y points. In this case one also needs to include other normal forces that may come from self-contacts or from the container itself. (ii) *Geometrical self-avoidance.* Regions of the rod that are initially far away from each other may end up in close vicinity during the packing process. In order to account for the impossibility of self-intersections in such regions, we require that whenever two (or more) points become in contact, they are bound together sharing a common position whose global location is otherwise free to move. Also, extended regions of contact are described by a new C or S curve whose thickness is adjusted according to the number of layers of which this region is made up.

The numerical resolution involves a shooting and branch tracking method. We start with a set of $5n$ shooting parameters: $\{\phi_i, \kappa_i, \kappa_i', a_i, \ell_i\}_{i=1,\ldots,n}$, where ϕ stands for the angle of the tangent to the rod with a constant direction ($d\phi/ds = \kappa$) and ℓ_i is the length between two consecutive Y points. Some of these parameters can be derived directly from the boundary conditions specified above, otherwise initial guesses are made for the remaining ones. The difference between their values and the desired boundary values at the other end of the integration interval is set up as a function which zeros are found with a Newton method. Eventually, this procedure yields the configurations of the sheet from which the corresponding mean pressures on the container can be extracted.

Now we describe the successive phases leading to the generation of spirals during the packing process. We compare the experiments and the numerics as the ratio between the excess perimeter of the cylindrical sheet and the perimeter of the container $\epsilon = (Z - R)/R = (L - 2\pi R)/2\pi R$ is increased. For low confinements, a symmetrical fold [Fig. 2(a) and 2(b)] grows inwards until its extremities become diametrically opposed. A first bifurcation occurs at

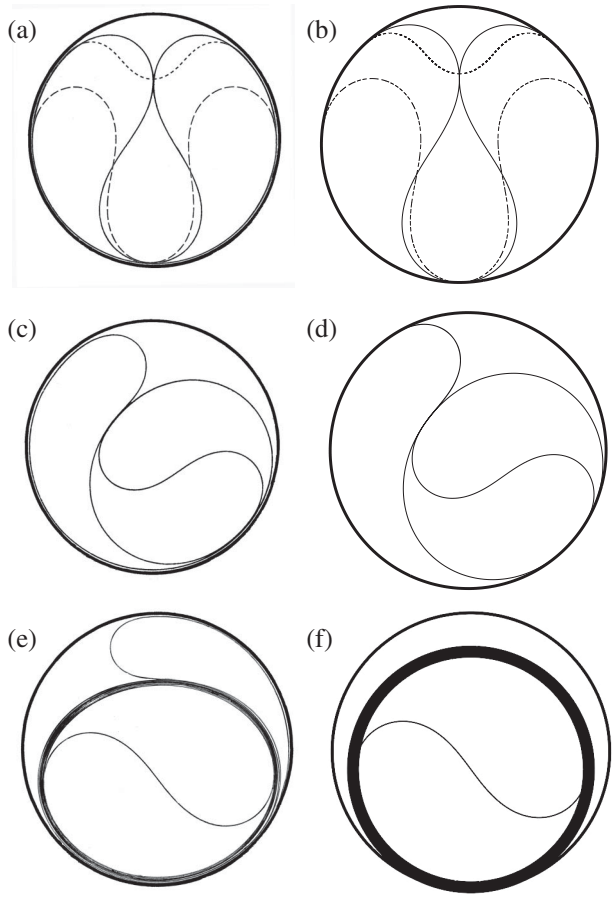

FIG. 2. Configurations for cylindrical packing. Experiments (left) and numerics (right) are almost indistiguishable. (a), (b) Symmetric configurations with no self-contact ($\epsilon = 0.016$, short dashed line), one self-contact point ($\epsilon = 0.31$, continuous line), and two self-contact points ($\epsilon = 0.66$, long dashed line). (c), (d) First asymmetric configuration for $\epsilon = 0.85$. The S curve and the surrounding C curves form a yin-yang-like pattern. (e) Yin-yang pattern at high confinement $\epsilon = 9.4$. The thick C curves are formed of 10 layers. (f) Numerical shape of the S curve in the yin-yang pattern for very large confinements. In this case, the C curves form a rigid circular effective container.

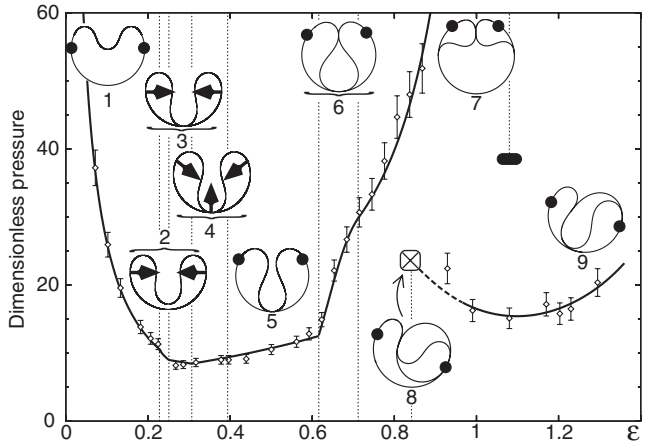

FIG. 3. Mean pressure as a function of confinement for cylindrical packing. The pressure is given in units of B/R^3. Diamonds correspond to experimental measurements and lines to theoretical results. The dashed line corresponds to metastable asymmetric configurations reflecting the hysteretic character of the transition; the cross signals a termination of the asymmetric branch. Vertical dashed lines correspond to separations between different types of numerical configurations shown as insets numbered from 1 to 9. Single contacts with the container are labeled with force vectors; lineic contacts with the container are delimited by disks.

$\epsilon = 0.23$ and the contact between the sheet and the container reduces to two diametrically opposed points (inset 2 of Fig. 3). Then at $\epsilon = 0.25$, a first self-contact appears between the inward fold and the C curve. As ϵ is increased, this contact point is driven back toward the disk and finally reaches it, thereby creating rather peculiar configurations displaying 3 localized contacts with their container, which exist in the range $0.31 < \epsilon < 0.39$ (inset 4 of Fig. 3). This additional support leads to an increase in the external pressure although the gap between the two C curves and the disk is too thin to be observed experimentally. Eventually these C curves come back in contact with the container leaving only two symmetrical S curves connected through a contact point with the disk, for $0.39 < \epsilon < 0.62$ [Fig. 2(a) and 2(b)]. A second self-contact appears at $\epsilon = 0.62$ [Fig. 2(a) and 2(b)]. Above $\epsilon = 0.71$, the lower contact point flattens out into an extended zone of self-contact (inset 7 of Fig. 3). While configurations with an axis of symmetry disappear at $\epsilon = 1.04$, asymmetric configurations may appear above $\epsilon = 0.85$ [Fig. 2(c) and 2(d)]: a lower bump of one S curve suddenly dives into the convex part of the second S curve forcing the lower self-contact to slide away from its symmetrical position. The transition between the two types of configurations is thus hysteretic. At this point, we observe experimentally that the inner S curve begins to rotate surrounding itself by spiral layers of C curves [Fig. 1(c)]. While the size of the outer loop (formed by the remaining S curve) decreases, a yin-yang-like shape embedded in an effective spiral container promptly develops [Fig. 2(e)]. When multiple turns have been completed, the outermost layer of the C curves is almost a circle and the pattern is formed of an S curve surrounded by a spiral of pitch equal to the thickness of the sheet h. The shape of the S curve can easily be determined numerically and is shown in Fig. 2(f). The pressures computed numerically are in good agreement with the experimental values (Fig. 3).

In three dimensions, the uniform close packing of a rod yields an optimal helix with a pitch and a radius proportional to the thickness of the rod [18,19]. In two dimensions, we propose that the optimal packing of a rod yields a spiral of pitch equal to the thickness of the rod h, one of the rod extremities being at the center of the spiral. This tiling is optimal because the only unoccupied region is the core

of the spiral, which area is of the order of h^2. Indeed, this geometrical construction naturally arises in our experiments on cylindrical sheets. However, a yin-yang pattern [Fig. 2(e)] is found in the core because a cross section of the sheet does not have any extremity inside the core; moreover, the radius of the core is in general much larger than h because of the high elastic cost of bending the sheet on such a small scale.

Now we turn to the estimation of the pressure needed to maintain such a structure within a surface of area $S = \pi R^2$ in terms of the packing ratio $p = Lh/S$. The area of the core is approximately the difference between S and the area occupied by the sheet Lh. Therefore, the radius of the core is given by $R_c = \sqrt{(S - Lh)/\pi}$. Its bending energy is proportional to B/R_c:

$$E_{S\ \mathrm{curve}} = \alpha \frac{\sqrt{\pi} B}{\sqrt{S}} \frac{1}{\sqrt{1-p}}, \tag{2}$$

where $\alpha = 17.44$ is the nondimensioned energy of the S curve as found numerically [Fig. 2(f)]. Besides, the radius of curvature of the spiral increases by an amount of h each time a new layer surrounds the inner core:

$$\frac{1}{\kappa(\theta)} = \frac{h}{2\pi}\theta + \sqrt{\frac{S - Lh}{\pi}} \tag{3}$$

in terms of the polar angle θ. Integrating the square of the curvature κ, we obtain the elastic energy of the spiral:

$$E_{\mathrm{spiral}} = \frac{\pi B}{2h} \ln \frac{1}{1-p}. \tag{4}$$

From this, one can compute the total bending energy (per unit height) $E = E_{\mathrm{spiral}} + E_{S\ \mathrm{curve}}$ and thus the mechanical pressure $P = -\partial E/\partial S$,

$$P = \frac{\pi B}{2hS} \frac{p}{1-p} + \alpha \frac{\sqrt{\pi} B}{2S^{3/2}} \frac{1}{(1-p)^{3/2}}. \tag{5}$$

This expression matches a simple scaling $P \sim BL/S^2$ at low packing ratio ($p = Lh/S \ll 1$) to a nontrivial divergence when $p \sim 1$ because of the high energetic cost of the core. This equation successfully reproduces the experimental measurements for spiral configurations with packing ratios p as large as 15% (such as in Fig. 2(e)].

In this Letter we showed how spirals are generated from a sequence of bifurcations. In an ideal system we would expect only one spiral. However, in real situations, friction between layers of C curves kicks in for higher confinements and tends to freeze the C curves into an effective thicker and more rigid sheet. This creates effective containers within which the same sequence is repeated, generating new spiraling patterns. While the underlying individual pockets still grow in a spiral fashion, an apparently complex pattern emerges from this cascade of bifurcations [Fig. 1(b)]. Although we investigated a simplified geometry for packing, our results have a wider scope because they are based on the key ingredients of elasticity and self-avoidance. Indeed, for the more complex packing of 2D elastic sheets in 3D containers, a cut through a crumpled ball of paper yields 1D curves, the topology of which could correspond to an assembly of spirals. This is the subject of work in progress.

This work was partly supported by the Ministre de la Recherche-ACI Jeunes Chercheurs and by the EEC MechPlant NEST project. Laboratoire de Physique Statistique is associated with the CNRS (UMR No. 8550) and Universities Paris VI and Paris VII.

*Electronic address: arezki.boudaoud@lps.ens.fr

[1] H. Kobayashi, B. Kresling, and J. F. V. Vincent, Proc. R. Soc. B **265**, 147 (1998).
[2] J. H. Brackenbury, J. Zool. **232**, 253 (1994).
[3] P. K. Purohit, M. M. Inamdar, P. D. Grayson, T. M. Squires, J. Kondev, and R. Phillips, Biophys. J. **88**, 851 (2005)
[4] N. Kleckner, D. Zickler, G. H. Jones, J. Dekker, R. Padmore, J. Henle, and J. A. Hutchinson, Proc. Natl. Acad. Sci. U.S.A. **101**, 12 592 (2004).
[5] A. Lobkovsky, S. Gentges, H. Li, D. Morse, and T. Witten, Science **270**, 1482 (1995).
[6] F. Plouraboué and S. Roux, Physica (Amsterdam) **227A**, 173 (1996).
[7] M. Ben Amar and Y. Pomeau, Proc. R. Soc. A **453**, 729 (1997).
[8] S. Chaïeb, F. Melo, and J. C. Geminard, Phys. Rev. Lett. **80**, 2354 (1998).
[9] E. Cerda, S. Chaïeb, F. Melo, and L. Mahadevan, Nature (London) **401**, 46 (1999).
[10] A. Boudaoud, P. Patricio, Y. Couder, and M. Ben Amar, Nature (London) **407**, 718 (2000).
[11] K. Matan, R. B. Williams, T. Witten, and S. R. Nagel, Phys. Rev. Lett. **88**, 076101 (2002).
[12] D. L. Blair and A. Kudrolli, Phys. Rev. Lett. **94**, 166107 (2005).
[13] G. A. Vliegenthart and G. Gomper, Nat. Mater. **5**, 216 (2006).
[14] E. Sultan and A. Boudaoud, Phys. Rev. Lett. **96**, 136103 (2006).
[15] B. Roman and A. Pocheau, Europhys. Lett. **46**, 602 (1999).
[16] C. C. Donato, M. A. F. Gomes, and R. E. de Souza, Phys. Rev. E **67**, 026110 (2003).
[17] E. Cerda and L. Mahadevan, Proc. R. Soc. A **461**, 671 (2005).
[18] A. Maritan, C. Micheletti, A. Trovato, and J. R. Banavar, Nature (London) **406**, 287 (2000).
[19] S. Przybyl and P. Pieranski, Eur. Phys. J. E **4**, 445 (2001).